

Article

Synthesis of Ternary Cross-Linked MoS₂/WS₂/CdS Photocatalysts for Photocatalytic H₂ Production

Yuping Sun ¹, Binfen Wang ¹, Xiaoqiang Liu ¹, Li Gao ^{1,*} and Wenfeng Shangguan ^{2,*}

¹ College of Chemistry and Molecular Sciences, Henan University, Kaifeng 475004, China; syp1988588@163.com (Y.S.); 15536351129@163.com (B.W.); liuxq@henu.edu.cn (X.L.)

² Research Center for Combustion and Environmental Technology, Shanghai Jiao Tong University, Shanghai 200240, China

* Correspondence: gaoli@henu.edu.cn (L.G.); shangguan@sjtu.edu.cn (W.S.)

Abstract: Photocatalytic H₂ production provides an ideal way to alleviate the energy crisis and solve environmental problems. In this paper, the metallic MoS₂/WS₂ dual cocatalysts are prepared through the in situ growth of 1T-WS₂ on the surface of 1T-MoS₂ via a solvothermal method. The ternary cross-linked MoS₂/WS₂/CdS photocatalysts are finally constructed by growing CdS nanorods on MoS₂/WS₂ cocatalysts. The XRD and TEM results show that ternary cross-linked MoS₂/WS₂/CdS photocatalysts with close interfacial contact were successfully synthesized. The results of Photoluminescence (PL) and photoelectrochemical tests show that MoS₂/WS₂/CdS has the lowest hydrogen evolution overpotential and the highest charge separation efficiency. This is due to the synergistic effect between WS₂ and MoS₂, which further accelerates the transfer of photogenerated electrons and inhibits the recombination of carriers. The hydrogen evolution rate of the MoS₂/WS₂/CdS composite is 12.12 mmol·g⁻¹·h⁻¹, which is 4.57 times that of pristine CdS. The AQY at λ = 420 nm is 58.9%.

Keywords: photocatalyst; H₂ production; MoS₂/WS₂/CdS; synergistic effect



Citation: Sun, Y.; Wang, B.; Liu, X.; Gao, L.; Shangguan, W. Synthesis of Ternary Cross-Linked MoS₂/WS₂/CdS Photocatalysts for Photocatalytic H₂ Production. *Catalysts* **2023**, *13*, 1149. <https://doi.org/10.3390/catal13081149>

Academic Editors: Detlef W. Bahnemann and Jorge Bedia

Received: 26 June 2023

Revised: 15 July 2023

Accepted: 24 July 2023

Published: 25 July 2023



Copyright: © 2023 by the authors. Licensee MDPI, Basel, Switzerland. This article is an open access article distributed under the terms and conditions of the Creative Commons Attribution (CC BY) license (<https://creativecommons.org/licenses/by/4.0/>).

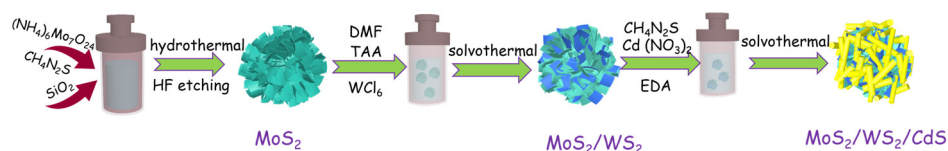
1. Introduction

Today, faced with the serious energy and environmental problems caused by the excessive use of fossil energy, there is an urgent need to develop green, economical and renewable energy. Photocatalytic water splitting to produce hydrogen has attracted extensive attention due to its ability to produce “green hydrogen” (without producing additional CO₂) [1–3]. CdS is one of the most studied visible-light photocatalysts because of its narrow band gap and appropriate band position. The band gap of CdS is 2.2~2.4 eV, and the light adsorption edge is 520~560 nm. Its conduction band (CB) and valence band (VB) potentials are -0.65 eV and +1.7 eV (NHE, pH = 0), respectively, exceeding the redox potential of water decomposition and providing almost perfect thermodynamic conditions [4–6]. However, the high recombination rate of photogenerated carriers on the surface of CdS results in low photocatalytic activity. Although Pt-based metal cocatalysts have shown good hydrogen evolution performance in photocatalytic reactions, their scarcity and high cost limit their application [7,8]. In recent years, researchers have found that some non-noble metals have suitable band gaps, which can significantly improve the photocatalytic performance of photocatalysts, meaning that they may represent alternative materials for noble metals [9].

Transition metal dichalcogenides (TMDs) have been found to possess high catalytic hydrogen evolution performance due to their unique two-dimensional layered structure, thus becoming a very promising alternative to precious metals. WS₂ and MoS₂ are typical transition metal disulfides in which the metal layer and the S layer are bonded by a weak van der Waals force, which is more adjustable than the covalently bonded structure [10–12]. Both WS₂ and MoS₂ have two different phases: a triangular prism (2H) and a metal octahedron (1T). Compared with the 2H phase, the 1T phases of WS₂ and MoS₂ are metallic and have low charge transfer resistance and highly active S vacancies, making them

more conducive to the hydrogen evolution reaction. Moreover, theoretical calculation and experimental results revealed that S atoms on exposed edges of MoS₂/WS₂ possessed strong attraction to H⁺, which was beneficial for hydrogen generation. Kim et al. [13] synthesized MoS₂ thin films on a target substrate via a chemical vapor deposition process for hydrogen evolution. The results show that compared with 2H-MoS₂, 1T-MoS₂ can significantly improve the hydrogen evolution performance of photocatalysts. In addition, as reported, the formation of dual cocatalysts by constructing heterojunctions on the cocatalyst surface can further improve the cocatalytic performance. Xiang et al. [14] synthesized a thin layer of WS₂/graphene cocatalyst through the in situ growth of WS₂ on the surface of graphene via a hydrothermal method. Due to a strong interaction between CdS, WS₂ and graphene, the photogenerated electrons generated by CdS are transferred to graphene and WS₂ to improve the photocatalytic activity. Zhang et al. [15] prepared WS₂/WO₃/g-C₃N₄ composites using a hydrothermal method. WS₂/WO₃ grew along the surface of g-C₃N₄, which accelerated the transmission of electrons. The hydrogen production efficiency of WS₂/WO₃/g-C₃N₄ composites was six times that of g-C₃N₄.

In this article, 1T-MoS₂ was first prepared via a hydrothermal method, and then 1T-WS₂ was grown in situ on the surface of 1T-MoS₂ using a solvent method to form MoS₂/WS₂ cocatalysts. Finally, ternary cross-linked MoS₂/WS₂/CdS photocatalysts were prepared through growing CdS nanorods on the surface of MoS₂/WS₂ using a solvothermal method (Scheme 1). Due to the Schottky junction between CdS, WS₂, and MoS₂, the photogenerated electrons generated from CdS can quickly transfer to the surface of MoS₂ through WS₂, which increases the space distance between electrons and holes and facilitates the separation of carriers. In addition, the close interfacial contact that originated from the cross-linked structure further facilitates charge transfer from CdS to WS₂ and MoS₂. The hydrogen evolution rate of the 4% MoS₂/WS₂/CdS composite reaches 12.12 mmol·g⁻¹·h⁻¹, and the apparent quantum yield (AQY) at λ = 420 nm is about 58.9%.



Scheme 1. Schematic illustration of the synthesis of MoS₂/WS₂/CdS composites.

2. Results

The crystal structure of the samples was studied using XRD. As shown in Figure 1a, the diffraction peaks at 9.9°, 32.6° and 57.5° of MoS₂ correspond to the (002), (100) and (110) planes of the 1T phase (1T-MoS₂), respectively [16,17]. From the XRD pattern of WS₂, it can be observed that there are three obvious diffraction peaks located at 9.5°, 18.6° and 32.5°, respectively, corresponding to the (002), (004) and (100) planes of the 1T-WS₂ [18]. The XRD pattern of MoS₂/WS₂ shows an obvious diffraction peak at 9.5° belonging to the (002) plane of 1T-WS₂. Since the position of the diffraction peak of the (002) plane of MoS₂ almost coincides with that of 1T-WS₂, it is difficult to observe the diffraction peak of the (002) plane of MoS₂ due to the disturbance of the strong peak of the (002) plane of 1T-WS₂. In addition, compared with the diffraction peak of the (002) plane of pristine WS₂ (9.5°), the diffraction peak of the (002) plane of WS₂ in MoS₂/WS₂ is slightly shifted to a smaller angle of 9.37°, which is probably due to the Mo atoms doping in the interlayer spacing of WS₂. From Figure 1b, obvious diffraction peaks can be observed at 25.2°, 44° and 52.1° in the XRD pattern of CdS, which correspond to the (100), (110) and (112) planes of hexagonal CdS, respectively [19]. The XRD patterns of MoS₂/CdS and MoS₂/WS₂/CdS are basically consistent with those of CdS, which is attributed to the low loading of MoS₂ and MoS₂/WS₂. The effect of cocatalyst loading on the light absorption performance of photocatalysts was investigated via UV-visible diffuse reflectance spectroscopy (UV-vis DRS). As shown in Figure 1c, the absorption edge of CdS is located at about 553 nm, corresponding to a band gap of 2.4 eV obtained using the Tauc plot (Figure 1d) [20].

After the introduction of MoS₂ and MoS₂/WS₂, the absorption edge of the photocatalytic materials is unchanged. However, the MoS₂/WS₂/CdS composite exhibits a stronger absorption than pristine CdS in the range of visible light (530~580 nm), which confirms that the loading of MoS₂/WS₂ promotes the visible light absorption performance of CdS, thus improving the photocatalytic hydrogen evolution activity.

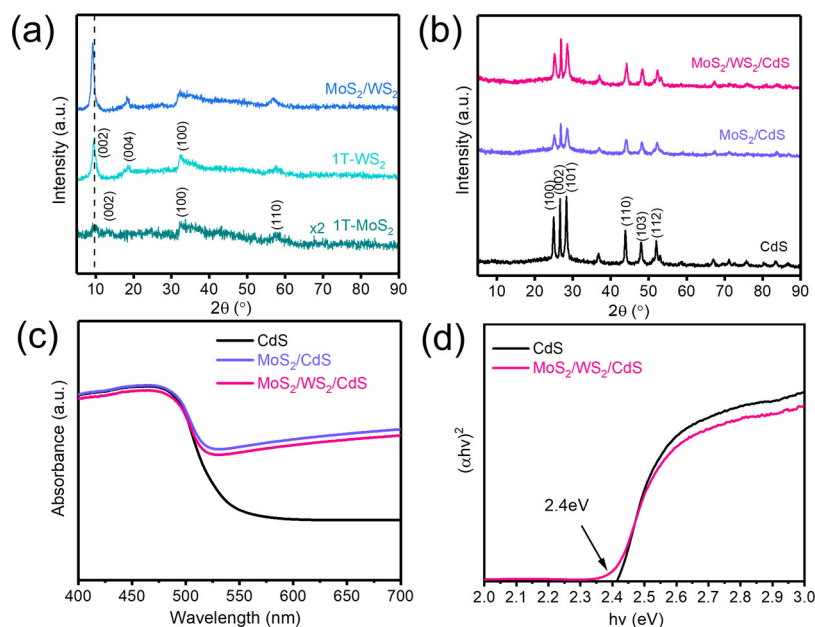


Figure 1. XRD patterns of (a) 1T-MoS₂, 1T-WS₂ and MoS₂/WS₂; (b) XRD patterns and (c) DRS spectra of CdS, MoS₂/CdS and MoS₂/WS₂/CdS; (d) Tauc plot curves of CdS and MoS₂/WS₂/CdS.

The morphology and structure of MoS₂, MoS₂/WS₂ and MoS₂/WS₂/CdS composites were analyzed using SEM and TEM. As shown in Figure 2a, the prepared 1T-MoS₂ is a microsphere aggregated by nanosheets with a size of about 500 nm. After loading 1T-WS₂, MoS₂/WS₂ is still a microsphere structure stacked by nanosheets (Figure 2b). From the TEM image of MoS₂/WS₂/CdS (Figure 2c), the rod-like CdS is tightly wrapped with MoS₂/WS₂, which results in the close contact between CdS and MoS₂/WS₂. From the HRTEM image (Figure 2d), a lattice spacing of 0.995 nm can be observed, which belongs to the (002) plane of 1T-WS₂ [21]. The lattice spacing of the (002) crystal plane of 1T-WS₂ in MoS₂/WS₂/CdS is larger than that of 1T-WS₂ (0.94 nm) in MoS₂/WS₂, which may be due to the entry of Cd atoms into the lattice of WS₂ during the formation of CdS. The lattice spacing belonging to 1T-MoS₂ was not found in TEM, which is due to the packaging of 1T-WS₂. Additionally, the lattice spacing of 0.35 nm belonging to the (100) plane of CdS can also be observed [22], indicating that CdS is successfully loaded on the surface of MoS₂/WS₂. The mapping (Figure 2e) shows Cd, S, Mo and W elements, indicating that the ternary cross-linked MoS₂/WS₂/CdS photocatalyst with close interfacial contact was prepared successfully.

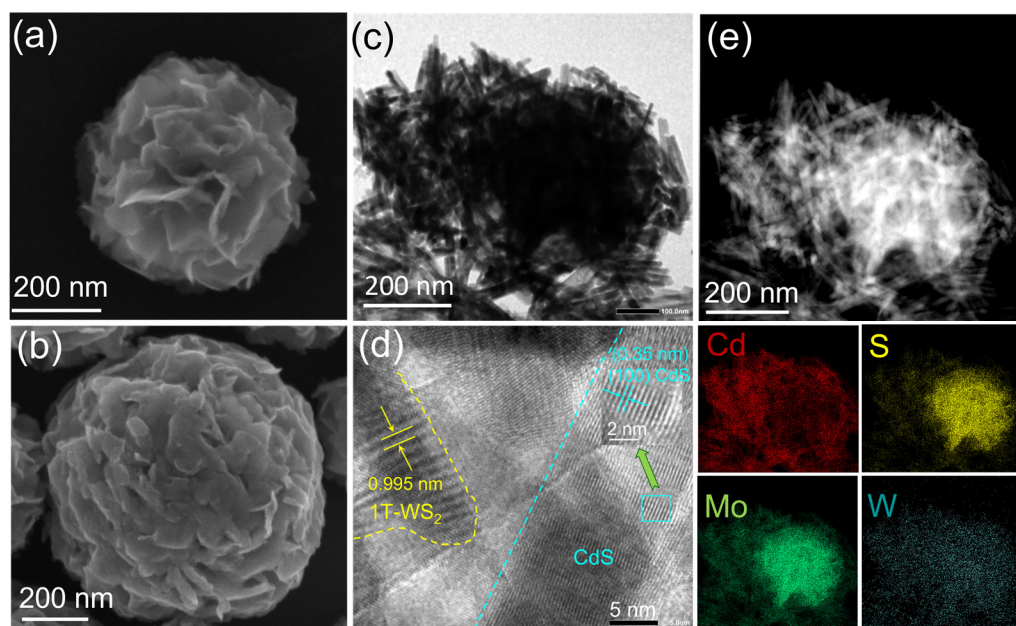


Figure 2. SEM images of (a) MoS₂ and (b) MoS₂/WS₂; (c) TEM, (d) HRTEM and (e) EDX mapping of MoS₂/WS₂/CdS.

The element composition and chemical states of MoS₂/WS₂/CdS were examined via XPS. As shown in Figure 3, the characteristic element peaks belonging to MoS₂, WS₂ and CdS can be observed from the XPS survey spectra. In the HRXPS spectra of Cd 3d, the peaks at 405.8 eV and 412.5 eV belong to 3d_{5/2} and 3d_{3/2} of Cd²⁺, respectively [23]. In the HRXPS spectra of Mo 3d, the peaks at 228.0 eV and 232.5 eV correspond to 3d_{5/2} and 3d_{3/2} of Mo of 1T-MoS₂, and the peaks at 229.2 eV and 233.5 eV correspond to 2H-MoS₂, indicating that there is a small amount of 2H-MoS₂ in the synthesized MoS₂, and the peak belonging to S 2s can be observed at 226.5 eV [24,25]. It can be clearly observed from the XPS spectrum of W 4f that two peaks appear at 30.8 eV and 34.0 eV, which are very consistent with the 4f_{7/2} and 4f_{5/2} of W⁴⁺ of 1T-WS₂, indicating that 1T-WS₂ is successfully grown on the surface of 1T-MoS₂, which is consistent with the XRD results. Similarly, the appearance of peaks at 31.9 eV and 35.9 eV suggests the presence of 2H-WS₂, and the peak at 37.7 eV belongs to the peak of the oxidation peak of W⁶⁺ [26–28]. S 2p contains S 2p_{3/2} and S 2p_{1/2} orbitals, in which the binding energies of 162.3 eV and 163.6 eV match those of S²⁻ [27]. The XPS results further confirm the synthesis of MoS₂/WS₂/CdS.

The photocatalytic hydrogen evolution activity of the samples was tested under 300 W ($\lambda > 420$ nm) Xe lamp irradiation. As shown in Figure 4, the photocatalytic hydrogen evolution rate of CdS is only 2.65 mmol·g⁻¹·h⁻¹, which is due to the lack of active sites. The photogenerated carriers of CdS quickly recombine on the surface instead of reducing protons to produce hydrogen due to the high overpotential of hydrogen evolution on the surface of CdS. After the introduction of MoS₂, the photocatalytic hydrogen evolution rate increased to 8.78 mmol·g⁻¹·h⁻¹. This is because the photogenerated electrons generated by CdS will be quickly transferred to the surface of MoS₂ due to the difference in Fermi level, thereby improving the separation efficiency of photogenerated charges. Interestingly, after loading the dual cocatalyst MoS₂/WS₂, the hydrogen evolution rate of the ternary cocatalyst MoS₂/WS₂/CdS was further improved. When the loading amount is 4%, the hydrogen evolution rate of the 2:1 MoS₂/WS₂/CdS composite reaches 12.12 mmol·g⁻¹·h⁻¹, which is 4.57 times that of CdS. Benefitting from the heterojunction between MoS₂ and WS₂, the photogenerated electrons generated by CdS are transferred to WS₂ and then quickly transferred to MoS₂, thereby synergistically improving the photogenerated charge separation efficiency and photocatalytic hydrogen evolution activity.

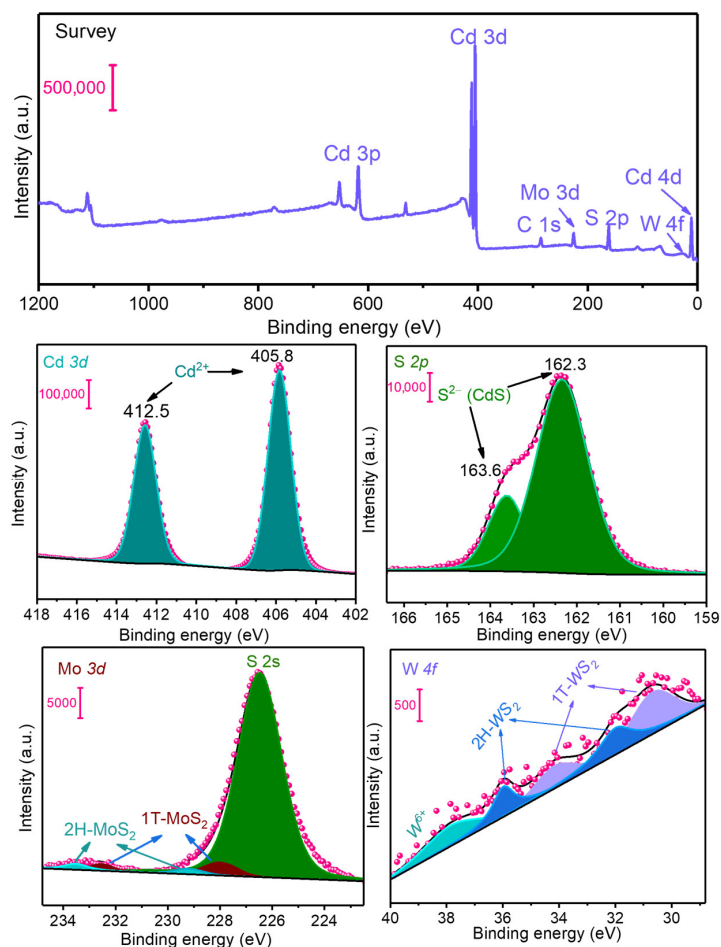


Figure 3. XPS survey spectrum of $\text{MoS}_2/\text{WS}_2/\text{CdS}$ and HRXPS spectra of Cd 3d, Mo 3d, W 4f and S 2p.

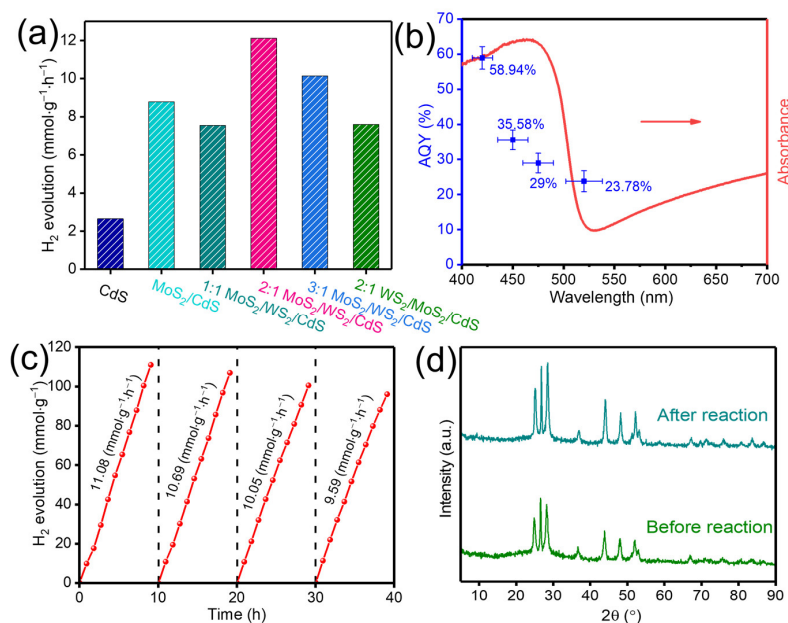


Figure 4. (a) H₂ evolution rates of CdS, MoS₂/CdS, MoS₂/WS₂/CdS and WS₂/MoS₂/CdS; (b) single wavelength AQYs and (c) cyclic experiment of 2:1 MoS₂/WS₂/CdS toward H₂ evolution; (d) XRD patterns of 2:1 MoS₂/WS₂/CdS before and after reaction for 40 h.

In addition, the mass ratio of MoS₂ to WS₂ also affects the cocatalytic performance of MoS₂/WS₂. When the mass ratio of WS₂ in MoS₂/WS₂ is increased (1:1) or decreased (3:1), the photocatalytic hydrogen evolution rates of the ternary MoS₂/WS₂/CdS are significantly reduced. This may be because when WS₂ grows too thick on the surface of MoS₂, it is difficult for photogenerated electrons to quickly transport to MoS₂ through WS₂, thus reducing a charge separation efficiency and resulting in a decrease in the photocatalytic hydrogen evolution rate. When the loading amount of WS₂ is too low, the synergistic effect of MoS₂/WS₂ is weakened, thus reducing the hydrogen evolution activity. In addition, to explore the electron transfer pathway, the effects of the growth order of WS₂ and MoS₂ on the photocatalytic hydrogen evolution activity were investigated. MoS₂/WS₂ and WS₂/MoS₂ cocatalysts were synthesized, respectively, and CdS was grown in situ on the surface of the two cocatalysts for photocatalytic hydrogen production. The results show that the photocatalytic hydrogen evolution activity of WS₂/MoS₂/CdS is not only lower than that of MoS₂/WS₂/CdS, but also lower than that of MoS₂/CdS. This result suggests that the photogenerated electrons are quickly transferred from CdS to MoS₂ and then further transferred to WS₂. On the contrary, the electrons transferred from CdS to WS₂ are difficult to transfer to MoS₂.

To obtain comparable hydrogen evolution performance, the hydrogen evolution rates and corresponding AQYs of 2:1 MoS₂/WS₂/CdS at different wavelengths were investigated, as shown in Figure 4b and Table 1. At $\lambda = 420$ nm, the AQY of 2:1 MoS₂/WS₂/CdS is about 58.9%, which indicates that MoS₂/WS₂ has excellent cocatalytic performance. To explore the photocatalytic stability of MoS₂/WS₂/CdS, the cyclic experiment of the 2:1 MoS₂/WS₂/CdS catalyst was carried out. As shown in Figure 4c, during the 40 h continuous reaction (four cycles), the hydrogen evolution rate only slightly decreased from 11.08 mmol·g⁻¹·h⁻¹ to 9.59 mmol·g⁻¹·h⁻¹, which was attributed to the consumption of lactic acid. Moreover, the XRD spectra of MoS₂/WS₂/CdS before and after the reaction did not change (Figure 4d), indicating that the photocatalyst has high structural stability.

Table 1. Main data for obtaining AQYs of 2:1 MoS₂/WS₂/CdS under different wavelengths.

Wavelength	I (W·cm ⁻¹)	ⁿ H ₂ ($\mu\text{mol}\cdot\text{h}^{-1}$)	N _p ^a	N _H ^b	AQY
420 nm	21.73	178.3	1.01×10^{17}	5.96×10^{16}	58.9%
450 nm	40.15	213.1	2.00×10^{17}	7.13×10^{16}	35.6%
470 nm	44.91	205.1	2.36×10^{17}	6.86×10^{16}	29.0%
520 nm	38.44	157.6	2.22×10^{17}	5.27×10^{16}	23.8%

^a The number of photons. ^b The number of protons.

The kinetics of photogenerated carrier separation was studied through PL spectroscopy and photoelectrochemical tests. Considering the recombination process of photoinduced electrons and holes, the generated energy is emitted in the form of fluorescence [29]. Therefore, the separation efficiency of photogenerated carriers can be reflected by the PL intensity of the sample. As shown in Figure 5a, the PL intensity of CdS is the strongest, implying the strongest charge recombination. After loading the MoS₂ cocatalyst, the PL intensity of the MoS₂/CdS becomes weaker. Obviously, the MoS₂/WS₂/CdS possesses the weakest PL intensity, suggesting that the MoS₂/WS₂ cocatalyst further promotes the separation of photogenerated electron–hole pairs [30]. To explore the reason why MoS₂/WS₂ functions as an active site for hydrogen evolution, linear sweep voltammetry (LSV), electrochemical impedance spectroscopy (EIS) and transient photocurrent response (i-t) were performed. From the LSV curves of the sample (Figure 5b), CdS exhibits a high onset potential for H₂ evolution and a lower reduction current density, indicating that there is a high hydrogen evolution overpotential and slow hydrogen evolution kinetics on the CdS surface [31]. The loading of MoS₂ and MoS₂/WS₂ can reduce the onset potential for H₂ evolution, indicating that the H₂ evolution reaction is more likely to occur on the surface of cocatalysts. From the EIS plots of the samples (Figure 5c), the semi-circular diameter of the

loaded CdS is smaller than that of pristine CdS, indicating that the interfacial resistance of electron transfer becomes smaller [32,33]. The semi-circular diameter of MoS₂/WS₂/CdS is smaller than that of MoS₂/CdS, indicating that the synergistic effect of MoS₂/WS₂ further promotes the hydrogen evolution kinetics. In addition, from the i-t curves of the photocatalysts (Figure 5d), it can be seen that, compared with CdS, loaded CdS shows stronger photocurrent density and MoS₂/WS₂/CdS has the strongest photocurrent density, further indicating that the synergistic effect of MoS₂/WS₂ promotes the separation efficiency of carriers.

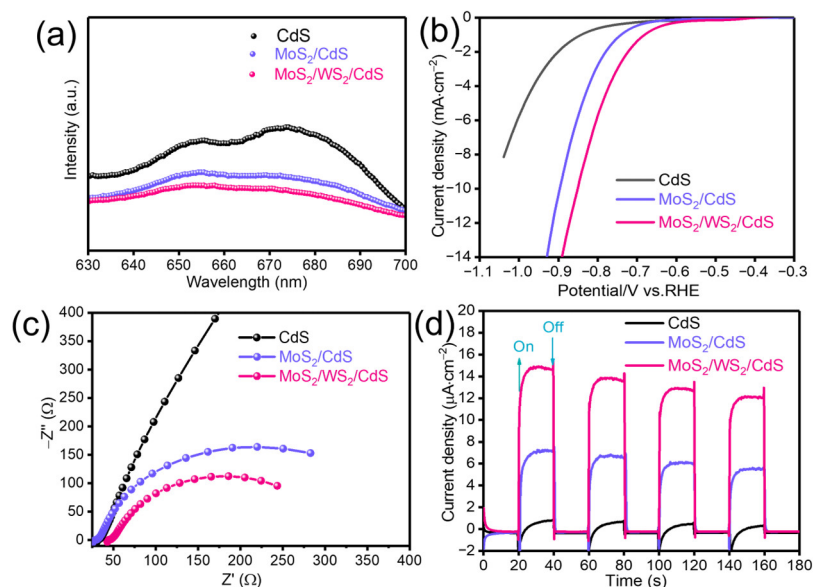


Figure 5. (a) PL spectra, (b) LSV curves, (c) EIS plots and (d) photocurrent response (i-t) of CdS MoS₂/CdS and MoS₂/WS₂/CdS.

The lifetime of photogenerated carriers of the MoS₂/WS₂/CdS photocatalyst was studied using the time-resolved photoluminescence (TRPL) technique. The average PL lifetime can be used to reflect the separation efficiency of photogenerated electrons and holes [34]. The double exponential function was used to fit the emission decay curve as shown in Figure 6, and the average lifetimes (τ_{ave}) of the CdS and MoS₂/WS₂/CdS were calculated. The lifetime of MoS₂/WS₂/CdS (3.45 ns) is shorter than that of CdS (4.25 ns), implying that the photogenerated electrons generated by CdS quickly transfer to MoS₂/WS₂, which improves the separation rate of electrons and holes, thereby enhancing the photocatalytic hydrogen evolution activity [35,36].

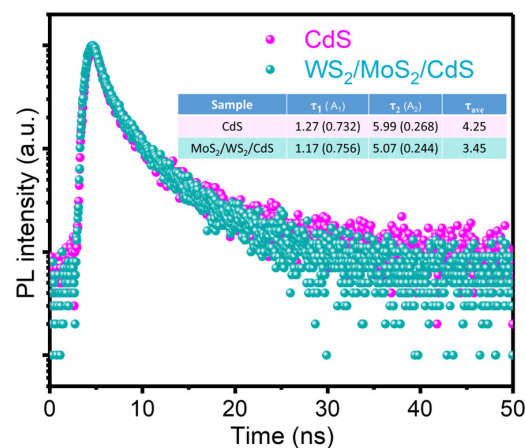


Figure 6. TRPL spectra and lifetimes of CdS and MoS₂/WS₂/CdS.

To better explain the charge separation dynamics of $\text{MoS}_2/\text{WS}_2/\text{CdS}$, the flat band potentials of 1T- WS_2 , MoS_2/WS_2 and CdS were measured using the Mott–Schottky technique (Figure 7). The M–S curves of CdS, 1T- WS_2 and 1T- MoS_2 have a positive slope, indicating that they are n-type semiconductors with flat band potentials of -1.4 V, -0.4 V and -0.4 V, respectively [37,38]. The flat band potential of 1T MoS_2 is very close to that of 1T WS_2 (-0.4 V), which can be attributed to the similar structure of 1T MoS_2 and 1T WS_2 . In addition, the flat band potential of MoS_2/WS_2 equals that of 1T- WS_2 . For an n-type semiconductor, since the flat band potential approaches the CB potential of the catalyst, the CB potentials of CdS and MoS_2/WS_2 are -1.4 V and -0.4 V, respectively [39,40]. Based on the above results, the possible mechanism of photocatalytic hydrogen evolution on $\text{MoS}_2/\text{WS}_2/\text{CdS}$ was proposed (Figure 7c). Under the excitation of light, electrons in VB of CdS are excited to the CB, and then migrate to the surface of CdS to reduce protons to H_2 . The holes remain on the VB and are consumed by the sacrificial reagent. However, due to the lack of active sites on the surface of CdS, most of the electrons and holes are rapidly recombined, which results in low photocatalytic activity. After loading MoS_2/WS_2 , since the CB potential of WS_2 is lower than that of CdS, the electrons on the CB of CdS are easily transferred to the surface of WS_2 through the close contact interface between WS_2 and CdS. Importantly, due to the Schottky junction between WS_2 and MoS_2 , some of the photogenerated electrons on WS_2 further migrate to the surface of MoS_2 . Benefiting from the synergistic effect between WS_2 and MoS_2 , the separation efficiency of carriers is improved, thereby enhancing the photocatalytic hydrogen evolution activity.

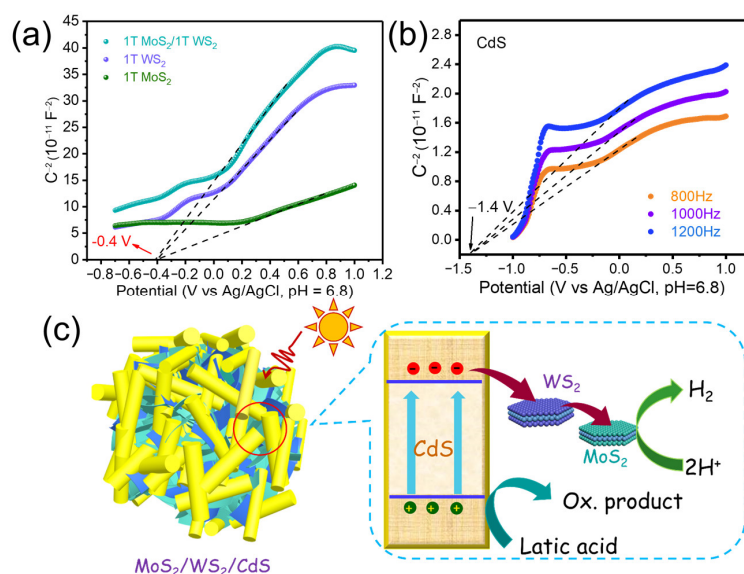


Figure 7. Mott–Schottky curves of (a) 1T- WS_2 , 1T MoS_2 , MoS_2/WS_2 and (b) CdS; (c) illustration showing the mechanism for enhanced photocatalytic activity over $\text{MoS}_2/\text{WS}_2/\text{CdS}$.

3. Experimental

3.1. Preparation of Photocatalysts

3.1.1. Preparation of 1T- MoS_2

To prepare 1T- MoS_2 , 0.284 g of $(\text{NH}_4)_6\text{Mo}_7\text{O}_{24}\cdot 4\text{H}_2\text{O}$ and 0.568 g of $\text{CH}_4\text{N}_2\text{S}$ were dissolved in 30 mL of deionized water, and 1 g of SiO_2 was slowly added to the above solution under stirring. Then, the mixture was put into a 45 mL polytetrafluoroethylene-lined autoclave and maintained at 210 °C for 18 h. The obtained black solid was fully washed with ethanol and water and dried at 60 °C for 12 h to form 1T- $\text{MoS}_2/\text{SiO}_2$. An appropriate amount of HF aqueous solution was added to the dried black solid to remove SiO_2 . After soaking for 6 h, the black 1T- MoS_2 solid was obtained.

3.1.2. Preparation of MoS₂/WS₂

MoS₂/WS₂ cocatalysts were synthesized by means of a solvothermal method. Typically, 0.2 g of MoS₂ was ultrasonically dispersed in 25 mL of DMF, and then 0.28 g of WCl₆ and 0.529 g of TAA were dissolved in the mixture. After ultrasonic treatment for 0.5 h, the mixture was transferred into a 45 mL polytetrafluoroethylene-lined autoclave and maintained at 200 °C for 24 h. The MoS₂/WS₂ black solid with a mass ratio of 2:1 was obtained by washing it with deionized water and ethanol. By changing the mass ratio of 1T-MoS₂ and 1T-WS₂, 1:1 MoS₂/WS₂ and 3:1 MoS₂/WS₂ were prepared, respectively.

3.1.3. Preparation of MoS₂/WS₂/CdS

The MoS₂/WS₂/CdS photocatalysts were obtained by means of the in situ growth of rod-like CdS on MoS₂/WS₂ using a solvothermal method. In this process, 0.0376 g of MoS₂/WS₂ (2:1) was ultrasonically dispersed in 48 mL of C₂H₈N₂ (EDA). Then, 1.54 g of Cd(NO₃)₂·4H₂O and 1.14 g of CH₄N₂S were added to the mixture. The mixture was transferred into a 45 mL polytetrafluoroethylene-lined autoclave and maintained at 160 °C for 48 h. The samples were washed with water and ethanol and dried at 40 °C in a vacuum oven to obtain 4% MoS₂/WS₂/CdS. Using the same method, 1:1 MoS₂/WS₂/CdS and 3:1 MoS₂/WS₂/CdS were prepared. As a comparison, MoS₂/CdS was prepared using the above method. In addition, MoS₂ was grown in situ on the surface of WS₂ via the above method to prepare 2:1 WS₂/MoS₂, and the then 2:1 WS₂/MoS₂/CdS photocatalyst was prepared as a comparison. Of note, in this paper, the loading amounts of the cocatalysts for all photocatalysts are 4%.

3.2. Characterization

The crystal structures of the samples were verified by collecting X-ray diffraction (XRD) patterns on a Bruker-AXS diffractometer with a Cu K α radiation source ($\lambda = 0.15406$ nm). The morphology of the photocatalysts was investigated using field emission scanning electron microscopy (FESEM) (Carl Zeiss GeminiSEM300, Zeiss, Oberkochen, Germany) and transmission electron microscopy (TEM, JEM-F200, JEOL, Tokyo, Japan). The UV-Vis diffuse reflection spectra (DRS) were acquired using an ultraviolet-visible-near-infrared spectrophotometer (UH4150, HITACHI, Tokyo, Japan). The surface electronic states were analyzed via X-ray photoelectron spectroscopy (XPS), which was performed with a Thermo Fisher Scientific K-Alpha spectrometer (Thermo Fisher Scientific, MA, USA) using a monochrome aluminum K α source ($h\nu = 1486.6$ eV). The sample was measured in a sample chamber. After the pressure was lower than 2.0×10^{-7} mbar, the sample was sent to the chamber for analysis using a 12 kV working voltage and 6 mA filament current. The HRXPS spectra of each element were fitted using XPSpeak 4.1 software based on Gauss–Lorentz curve fitting. The adventitious C 1s at 284.8 eV was applicable to calibrate the binding energy (BE) values. Photoluminescence (PL) and time-resolved PL (TRPL) spectra were recorded with a single photon counting spectrometer from an FLS980 fluorescence spectrometer with an excitation wavelength of 325 nm (Edinburgh Instruments, Livingston, UK).

3.3. Photoelectrochemical Measurements

The linear sweep voltammetry (LSV), photocurrent response (i-t) and electrochemical impedance spectroscopy (EIS) measurements were performed using a CH Instrument 760 E electrochemical workstation (Shanghai Chenhua Instrument, Shanghai, China), using a 0.5 mol·L⁻¹ Na₂SO₄ aqueous solution as an electrolyte. A platinum wire was used as a counter electrode and an Ag/AgCl electrode was used as a reference electrode. In this process, 5 mg of catalyst was dispersed in 1.5 mL of 0.1 wt% nafion solution to form a slurry. The working electrodes were prepared by coating the slurry onto ITO conducting glass (1 × 1 cm²) and dried at 25 °C overnight. A 300 W Xe lamp was used to provide visible light ($\lambda > 420$ nm). The Mott–Schottky (M-S) curve was measured on a CHI760E electrochemical workstation. The working electrodes were prepared by coating the slurry onto a glassy carbon electrode (3 mm diameter, 0.07 cm²) and dried at 25 °C overnight.

3.4. Photocatalytic Performance Evaluation System

The reaction was carried out in a 350 mL reactor that was kept at 25 °C via the circulation of cooling water. The photocatalytic hydrogen evolution rates were tested under 300 W ($\lambda > 420$ nm) xenon lamp irradiation. Each 50 mg photocatalyst was ultrasonically dispersed in a 65 mL aqueous solution of lactic acid (20%). Before irradiation, the reactor was vacuumed using a vacuum pump. The hydrogen production performance was tested using a gas chromatograph. The amount of generated H₂ was tested at intervals of 1 h using an on-line GC (TCD detector, Ar as the carrier gas). The AQYs of the 4% MoS₂/WS₂/CdS photocatalyst at $\lambda = 420$ nm, 450 nm, 475 nm and 520 nm were examined using bandpass filters and an irradiatometer (CEL-NP2000) according to the equations below:

$$\begin{aligned} \text{AQY}(\%) &= \frac{\text{The rate of reacted electrons } (N_H)}{\text{The rate of incident photons } (N_P)} \times 100\% \\ &= \frac{\text{The rate of evolved H}_2 \text{ molecules} \times 2}{\text{The rate of incident photons}} \times 100\% \\ &= \frac{N_H}{N_P} \times 100\% = \frac{2 \times n_{H_2} \times L}{\frac{A \times I}{E}} \times 100\% = \frac{2 \times n_{H_2} \times L}{\frac{A \times I}{(hc/\lambda)}} \times 100\% \end{aligned}$$

where n_{H_2} is the evolution rate of hydrogen molecules, mol/s; L is the Avogadro constant, 6.02×10^{23} mol⁻¹; I is the irradiance at $\lambda = 400$ nm, 420 nm, 450 nm, and 520 nm, W·m⁻²; A is the illuminated area, m²; E is the photon energy, eV; h is the Plank's constant, 6.63×10^{-34} , J·s; and c is the speed of light, 3×10^8 m·s⁻¹.

4. Conclusions

The MoS₂/WS₂ cocatalyst was prepared by means of the in situ growth of 1T-WS₂ on the surface of 1T-MoS₂ via a solvothermal method. The ternary cross-linked MoS₂/WS₂/CdS photocatalysts with close interfacial contact were constructed by growing CdS nanorods on MoS₂/WS₂ using a solvothermal method. Benefiting from the excellent synergistic effect of MoS₂ and WS₂, the MoS₂/WS₂ cocatalyst further improves the separation efficiency of photogenerated electrons and holes and enhances the catalytic activity. The hydrogen evolution rate of 2:1 MoS₂/WS₂/CdS photocatalyst reaches 12.12 mmol·g⁻¹·h⁻¹, which is 4.57 times that of CdS, and the AQY at $\lambda = 420$ nm is 58.9%. This study provides an effective strategy for the construction of dual cocatalysts with high cocatalytic performance.

Author Contributions: Conceptualization, Y.S. and B.W.; methodology, B.W.; validation, Y.S. and B.W.; investigation, Y.S., B.W., X.L. and L.G.; resources, L.G. and W.S.; writing—original draft preparation, Y.S. and B.W.; writing—review and editing, X.L., L.G. and W.S.; supervision, X.L. and L.G.; project administration, W.S.; funding acquisition, W.S. All authors have read and agreed to the published version of the manuscript.

Funding: This research was funded by The Natural Science Foundation of China (21773153).

Data Availability Statement: The data presented in this study are available on request from the corresponding authors.

Conflicts of Interest: The authors declare no conflict of interest.

References

- Chi, J.; Jiang, Z.; Yan, J.; Larimi, A.; Wang, Z.; Wang, L.; Shangguan, W. Recent advancements in bismuth vanadate photoanodes for photoelectrochemical water splitting. *Mater. Today Chem.* **2022**, *26*, 101060. [[CrossRef](#)]
- Yan, Y.; Chen, Z.; Cheng, X.; Shi, W. Research Progress of ZnIn₂S₄-Based Catalysts for Photocatalytic Overall Water Splitting. *Catalysts* **2023**, *13*, 967. [[CrossRef](#)]
- He, Y.; Dai, X.; Ma, S.; Chen, L.; Feng, Z.; Xing, P.; Yu, J.; Wu, Y. Hydrothermal preparation of carbon modified KNb₃O₈ nanosheets for efficient photocatalytic H₂ evolution. *Ceram. Int.* **2020**, *46*, 11421–11426. [[CrossRef](#)]
- Shen, R.; Ren, D.; Ding, Y.; Guan, Y.; Ng, Y.; Zhang, P.; Li, X. Nanostructured CdS for efficient photocatalytic H₂ evolution: A review. *Sci. China Mater.* **2020**, *63*, 2153–2188. [[CrossRef](#)]
- Mirsalari, S.A.; Nezamzadeh-Ejehieh, A.; Massah, A.R. A designed experiment for CdS-AgBr photocatalyst toward methylene blue. *Environ. Sci. Pollut. Res.* **2022**, *29*, 33013–33032. [[CrossRef](#)]

6. Bie, C.; Fu, J.; Cheng, B.; Zhang, L. Ultrathin CdS nanosheets with tunable thickness and efficient photocatalytic hydrogen generation. *Appl. Surf. Sci.* **2018**, *462*, 606–614. [[CrossRef](#)]
7. Cai, M.; Cao, S.; Zhuo, Z.; Wang, X.; Shi, K.; Cheng, Q.; Xue, Z.; Du, X.; Shen, C.; Liu, X.; et al. Fabrication of Ni₂P Cocatalyzed CdS Nanorods with a Well-Defined Heterointerface for Enhanced Photocatalytic H₂ Evolution. *Catalysts* **2022**, *12*, 417. [[CrossRef](#)]
8. Li, X.; Gao, Y.; Li, N.; Ge, L. In-situ constructing cobalt incorporated nitrogen-doped carbon/CdS heterojunction with efficient interfacial charge transfer for photocatalytic hydrogen evolution. *Int. J. Hydrogen Energy* **2022**, *47*, 27961–27972. [[CrossRef](#)]
9. Li, S.; Wang, L.; Li, Y.; Zhang, L.; Wang, A.; Xiao, N.; Gao, Y.; Li, N.; Song, W.; Ge, L.; et al. Novel photocatalyst incorporating Ni-Co layered double hydroxides with P-doped CdS for enhancing photocatalytic activity towards hydrogen evolution. *Appl. Catal. B* **2019**, *254*, 145–155. [[CrossRef](#)]
10. Coogan, Á.; Gun'ko, Y.K. Solution-based “bottom-up” synthesis of group VI transition metal dichalcogenides and their applications. *Mater. Adv.* **2021**, *2*, 146–164. [[CrossRef](#)]
11. Teo, W.Z.; Chng, E.L.; Sofer, Z.; Pumera, M. Cytotoxicity of exfoliated transition-metal dichalcogenides (MoS₂, WS₂, and WSe₂) is lower than that of graphene and its analogues. *Chem. Eur. J.* **2014**, *20*, 9627–9632. [[CrossRef](#)] [[PubMed](#)]
12. Anto Jeffery, A.; Nethravathi, C.; Rajamathi, M. Two-dimensional nanosheets and layered hybrids of MoS₂ and WS₂ through exfoliation of ammoniated MS₂ (M = Mo, W). *J. Phys. Chem. C* **2014**, *118*, 1386–1396. [[CrossRef](#)]
13. Zou, Y.; Guo, C.; Cao, X.; Zhang, L.; Chen, T.; Guo, C.; Wang, J. Synthesis of CdS/CoP hollow nanocages with improved photocatalytic water splitting performance for hydrogen evolution. *J. Environ. Chem. Eng.* **2021**, *9*, 106270. [[CrossRef](#)]
14. Xiang, Q.; Cheng, F.; Lang, D. Hierarchical layered WS₂/graphene-modified CdS nanorods for efficient photocatalytic hydrogen evolution. *ChemSusChem* **2016**, *9*, 996–1002. [[CrossRef](#)]
15. Zhang, X.; Yang, P.; Jiang, S. Horizontally growth of WS₂/WO₃ heterostructures on crystalline g-C₃N₄ nanosheets towards enhanced photo/electrochemical performance. *J. Nanostruct. Chem.* **2021**, *11*, 367–380. [[CrossRef](#)]
16. Zhang, Z.; Li, Q.; Qiao, X.; Hou, D.; Li, D. One-pot hydrothermal synthesis of willow branch-shaped MoS₂/CdS heterojunctions for photocatalytic H₂ production under visible light irradiation. *Chin. J. Catal.* **2019**, *40*, 371–379. [[CrossRef](#)]
17. Zhang, Y.; Guo, S.; Xin, X.; Song, Y.; Yang, L.; Wang, B.; Tan, L.; Li, X. Plasmonic MoO₂ as co-catalyst of MoS₂ for enhanced photocatalytic hydrogen evolution. *Appl. Surf. Sci.* **2020**, *504*, 144291. [[CrossRef](#)]
18. Ding, C.; Zhao, C.; Cheng, S.; Yang, X. Ultrahigh photocatalytic hydrogen evolution performance of coupled 1D CdS/1T-phase dominated 2D WS₂ nanoheterojunctions. *Chin. J. Catal.* **2022**, *43*, 403–409. [[CrossRef](#)]
19. Reddy, D.A.; Park, H.; Hong, S.; Kumar, D.P.; Kim, T. Hydrazine-assisted formation of ultrathin MoS₂ nanosheets for enhancing their co-catalytic activity in photocatalytic hydrogen evolution. *J. Mater. Chem. A* **2017**, *5*, 6981–6991. [[CrossRef](#)]
20. Feng, C.; Chen, Z.; Jing, J.; Sun, M.; Tian, J.; Lu, G.; Ma, L.; Li, X.; Hou, J. Significantly enhanced photocatalytic hydrogen production performance of g-C₃N₄/CNTs/CdZnS with carbon nanotubes as the electron mediators. *J. Mater. Sci. Technol.* **2021**, *80*, 75–83. [[CrossRef](#)]
21. Liang, Z.; Yang, S.; Wang, X.; Cui, H.; Wang, X.; Tian, J. The metallic 1T-phase WS₂ nanosheets as cocatalysts for enhancing the photocatalytic hydrogen evolution of g-C₃N₄ nanotubes. *Appl. Catal. B* **2020**, *274*, 119114. [[CrossRef](#)]
22. Su, L.; Luo, L.; Song, H.; Wu, Z.; Tu, W.; Wang, Z.; Ye, J. Hemispherical shell-thin lamellar WS₂ porous structures composited with CdS photocatalysts for enhanced H₂ evolution. *Chem. Eng. J.* **2020**, *388*, 124346. [[CrossRef](#)]
23. Chen, W.; Liu, X.; Wei, S.; Heng, Q.; Wang, B.; Liu, S.; Gao, L.; Mao, L. In situ growth of a-few-layered MoS₂ on CdS nanorod for high efficient photocatalytic H₂ production. *Front. Energy* **2021**, *15*, 752–759. [[CrossRef](#)]
24. Kim, H.U.; Kim, M.; Seok, H.; Park, K.Y.; Moon, J.Y.; Park, J.; An, B.S.; Jung, H.; Dravid, V.; Whang, D.; et al. Realization of wafer-scale 1T-MoS₂ film for efficient hydrogen evolution reaction. *ChemSusChem* **2021**, *14*, 1344–1350. [[CrossRef](#)] [[PubMed](#)]
25. Wang, S.; Li, Y.; Hu, Y.; Zhou, X.; Zhang, M.; Jia, X.; Lin, B.; Chen, G. One-step synthesis of 1T MoS₂ hierarchical nanospheres for electrocatalytic hydrogen evolution. *ACS Appl. Energy Mater.* **2022**, *5*, 11705–11712. [[CrossRef](#)]
26. Yi, J.; She, X.; Song, Y.; Mao, M.; Xia, K.; Xu, Y.; Mo, Z.; Wu, J.; Xu, H.; Li, H. Solvothermal synthesis of metallic 1T-WS₂: A supporting co-catalyst on carbon nitride nanosheets toward photocatalytic hydrogen evolution. *Chem. Eng. J.* **2018**, *335*, 282–289. [[CrossRef](#)]
27. Srinivaas, M.; Wu, C.Y.; Duh, J.G.; Wu, J. Highly rich 1T metallic phase of few-layered WS₂ nanoflowers for enhanced storage of lithium-ion batteries. *ACS Sustain. Chem. Eng.* **2019**, *7*, 10363–10370. [[CrossRef](#)]
28. Kim, M.J.; Jeon, S.J.; Kang, T.W.; Ju, J.M.; Yim, D.; Kim, H.I.; Park, J.; Kim, J.H. 2H-WS₂ quantum dots produced by modulating the dimension and phase of 1T-nanosheets for antibody-free optical sensing of neurotransmitters. *ACS Appl. Mater. Interfaces* **2017**, *9*, 12316–12323. [[CrossRef](#)]
29. Xiong, T.; Cen, W.; Zhang, Y.; Dong, F. Bridging the g-C₃N₄ interlayers for enhanced photocatalysis. *ACS Catal.* **2016**, *6*, 2462–2472. [[CrossRef](#)]
30. Heng, Q.; Wang, B.; Fan, X.; Chen, W.; Li, X.; Mao, L.; Shangguan, W. Enhanced photoreduction activity of CO₂ to CO over Ag-loaded mesoporous g-C₃N₄ (MCN) by promoting charge separation and CO₂ adsorption. *J. Alloys Compd.* **2022**, *920*, 165945. [[CrossRef](#)]
31. Li, F.; Yang, J.; Gao, J.; Liu, Y.; Gong, Y. Enhanced photocatalytic hydrogen production of CdS embedded in cationic hydrogel. *Int. J. Hydrogen Energy* **2020**, *45*, 1969–1980. [[CrossRef](#)]

32. Song, T.; Hou, L.; Long, B.; Ali, A.; Deng, G.J. Ultrathin MXene “bridge” to accelerate charge transfer in ultrathin metal-free 0D/2D black phosphorus/g-C₃N₄ heterojunction toward photocatalytic hydrogen production. *J. Colloid Interface Sci.* **2021**, *584*, 474–483. [[CrossRef](#)] [[PubMed](#)]
33. Chen, W.; Wang, Y.; Shangguan, W. Metal (oxide) modified (M = Pd, Ag, Au and Cu) H₂SrTa₂O₇ for photocatalytic CO₂ reduction with H₂O: The effect of cocatalysts on promoting activity toward CO and H₂ evolution. *Int. J. Hydrogen Energy* **2019**, *44*, 4123–4132. [[CrossRef](#)]
34. Heng, Q.; Ma, Y.; Wang, X.; Wu, Y.; Li, Y.; Chen, W. Role of Ag, Pd cocatalysts on layered SrBi₂Ta₂O₉ in enhancing the activity and selectivity of photocatalytic CO₂ reaction. *Appl. Surf. Sci.* **2023**, *632*, 157564. [[CrossRef](#)]
35. Lu, X.; Chen, W.; Yao, Y.; Wen, X.; Hart, J.; Tsounis, C.; Toe, C.; Scott, J.; Ng, Y. Photogenerated charge dynamics of CdS nanorods with spatially distributed MoS₂ for photocatalytic hydrogen generation. *Chem. Eng. J.* **2021**, *420*, 127709. [[CrossRef](#)]
36. Chen, R.; Wang, P.; Chen, J.; Wang, C.; Ao, Y. Synergetic effect of MoS₂ and MXene on the enhanced H₂ evolution performance of CdS under visible light irradiation. *Appl. Surf. Sci.* **2019**, *473*, 11–19. [[CrossRef](#)]
37. Li, L.; Gao, D.; Chen, F.; Wang, X.; Yu, H. Amorphization-crystallization synergism on MoS_x homojunction for boosting photocatalytic H₂ production of TiO₂ in alkaline medium. *Appl. Surf. Sci.* **2023**, *608*, 155173. [[CrossRef](#)]
38. Guan, Y.; Wu, J.; Lin, Y.; Liu, Q.; Qi, Y.; Pan, W.; He, P.; Qi, X.; Wang, R.; Ji, Z. Solvent-exfoliation of transition-metal dichalcogenide MoS₂ to provide more active sites for enhancing photocatalytic performance of BiOIO₃/g-C₃N₄ photocatalyst. *Appl. Surf. Sci.* **2019**, *481*, 838–851. [[CrossRef](#)]
39. Wang, B.; Sun, Y.; Fan, X.; Chen, W.; Liu, X.; Gao, L.; Mao, L. In situ growth of 1T-WS₂ on ultrathin Ti₃C₂T_x as a hybrid cocatalyst for enhancing the photocatalytic activity of CdS. *Appl. Surf. Sci.* **2023**, *615*, 156305. [[CrossRef](#)]
40. Fan, X.; Wang, B.; Heng, Q.; Chen, W.; Mao, L. Facile in-situ synthesis of a-NiS/CdS p-n junction with enhanced photocatalytic H₂ production activity. *Int. J. Hydrogen Energy* **2022**, *47*, 32531–32542. [[CrossRef](#)]

Disclaimer/Publisher’s Note: The statements, opinions and data contained in all publications are solely those of the individual author(s) and contributor(s) and not of MDPI and/or the editor(s). MDPI and/or the editor(s) disclaim responsibility for any injury to people or property resulting from any ideas, methods, instructions or products referred to in the content.